J Appl Electrochem (2010) 40:375–382
DOI 10.1007/s10800-009-0006-0

ORIGINAL PAPER

Hydrazine oxidation catalyzed by ruthenium hexacyanoferrate-modified glassy carbon electrode

Wendell M. Costa · Aldaléa L. B. Marques · Edmar P. Marques · Cicero W. B. Bezerra · Eliane R. Sousa · William S. Cardoso · Chaojie Song · Jiujun Zhang

Received: 29 May 2009 / Accepted: 21 August 2009 / Published online: 11 September 2009

Abstract A ruthenium (III) hexacyanoferrate (Ru(HCF)) film coated on a glassy carbon electrode was explored as an electrocatalyst for hydrazine oxidation. Surface cyclic voltammograms of Ru(HCF) film showed four reversible one-electron redox waves. Two, which corresponded to the redox processes of Ru(III)/Ru(IV) and Fe(II)/Fe(III), were identified to be responsible for the catalytic activity of hydrazine oxidation. Kinetic studies using potential scan rate dependency, Tafel plots, and rotating disk electrode technique found that this catalyzed hydrazine oxidation was a complete four-electron/four-proton process producing N_2, with the rate determining step possibly a one-electron process with a transfer coefficient (α) of $\sim$0.31–0.36. In addition, based on kinetic analysis and findings in the literature, we propose a possible reaction mechanism for catalyzed hydrazine oxidation in order to facilitate further understanding.

Keywords Ruthenium (III) hexacyanoferrate · Electrode modification · Electrocatalysis · Hydrazine oxidation

W. M. Costa · A. L. B. Marques (✉) · E. P. Marques · C. W. B. Bezerra · E. R. Sousa · W. S. Cardoso
Department of Technology Chemistry, Federal University of Maranhão, Av. dos Portugueses, S/N, Campus do Bacanga, São Luis, MA 65080-040, Brazil
e-mail: aldaleabrandes@hotmail.com

C. Song · J. Zhang
Institute for Fuel Cell Innovation, National Research Council of Canada, Vancouver, BC V6T 1W5, Canada

1 Introduction

Hydrazine is a compound of interest in the chemical and pharmaceutical industries, and has been used in a variety of applications, including as a chemical reducing agent, fuel, corrosion inhibitor and antioxidant, emulsifier, pesticide, and plant-growth regulator, as well as in dyes and explosives [1]. As a fuel in electrochemical energy devices such as fuel cells, hydrazine has drawn significant attention, particularly in the development of electrocatalysts capable of catalyzing its electrooxidation. The challenges arise mainly from overpotentials encountered in the direct electrooxidation of hydrazine at common electrode surfaces [2].

In the effort to develop electrocatalysts for hydrazine oxidation, various inorganic and organic materials have been explored, including quinizarine [2], chlorogenic acid [3], cobalt hexacyanoferrate [4], pyrocatechol violet (PCV) [5], cobalt phthalocyanine [6], cobalt tetraphenylporphyrin [7], nickel ferricyanide [8], coumestan [9], hybrid copper and cobalt hexacyanoferrate films [10], pyrogallol red, [11] and rhodium [12]. These approaches have demonstrated that when these materials were coated on inert electrode surfaces to form chemically modified electrodes (CMEs), the respective electrode could show an enhanced electron transfer rate and reduced overpotential toward hydrazine oxidation. Based on findings in the literature, we successfully fabricated some electrodes coated with a ruthenium hexacyanoferrate film, and found that these modified electrodes had strong catalytic activity toward hydrazine oxidation.

Transition metal hexacyanoferrates have been recognized as a highly important class of compounds for use as electrode surface modifiers [13]. In a metal hexacyanoferrate, there are two sets of redox couples: $Fe(CN)_6^{3+/4+}$ and $M^{n+}/M^{(n-1)+}$ (where M is the second metal). The presence of a second metal redox couple such as Ru^{3+}/Ru^{2+} not only can improve

the conductivity of the film, but also can prevent polynuclear hexacyanometalate dissolution [14–17]. In a catalyst application, the stability of the thin film on the electrode is crucial for electrode durability [18]; the fabrication method can play an important role in stabilizing the ruthenium hexacyanoferrate film [17, 19–22]. It has been demonstrated that the stability of electrochemically prepared films may be improved substantially if the hexacyanoferrate-modified electrode is electrochemical potential cycled in a freshly prepared acidic solution containing $RuCl_3$ [19]. This stabilizing effect has been attributed to the formation of binuclear metal centers [20], which had oxo-bridges between the Ru and Fe, thus: Ru–O–Fe [17–19, 22]. The film formed on the electrode could be considered a mix of ruthenium oxide and hexacyanoferrate ($RuO/Fe(CN)_6^{3-}$). In the literature, this ruthenium hexacyanoferrate film was found to be electrocatalytically active toward the oxidation of a variety of compounds, including dopamine and norepinephrine [23, 24]. However, to the best of our knowledge, no report has been published about the electrocatalytic activity of ruthenium hexacyanoferrate (Ru(HCF)) toward hydrazine oxidation.

In this study, we employed a drop evaporation/electrochemical potential cycling method and prepared Ru(HCF) films on glassy carbon electrodes. The electrocatalytic oxidation of hydrazine on such a Ru(HCF)-modified glassy carbon electrode was studied, using both cyclic voltammetry and rotating disk electrode techniques, in terms of the surface electrochemistry of Ru(HCF) and the kinetics of the electrooxidation of hydrazine.

2 Experimental

2.1 Chemicals and solutions

All the reagents used in this study were analytical grade and all solutions were prepared using ultrapure water, through a Barnstead Nanopure Lab Water System (Model 04741, Iowa, USA). A Britton–Robinson buffer system (BR) (CH_3COOH 0.04 mol L^{-1} + H_3BO_3 0.04 mol L^{-1} + H_3PO_4 0.04 mol L^{-1}), used to control pH, was added to 0.1 mol L^{-1} $NaClO_4$ as the supporting electrolyte. The initial pH of the solution was 1.8, and the desired pH was adjusted by the addition of 1.0 mol L^{-1} NaOH solution. The solutions were deaerated by purging with N_2. Test solutions were prepared by adding various specific amounts of 0.1 M hydrazine solution to the deaerated electrolyte solution.

2.2 Electrode preparation

The electrode was modified by the following procedure. The glassy carbon surfaces were polished successively with 1.0, 0.3, and 0.05 μm α-alumina suspensions on a microcloth polishing pad, then rinsed with water and sonicated for a few minutes in doubly distilled water. Then an aliquot (2.5–10 μL) of a ruthenium (III) hexacyanoferrate mixed solution containing 1×10^{-3} mol L^{-1} $K_3[Fe(CN)_6]$ and 1×10^{-3} mol L^{-1} $RuCl_3 \cdot 3H_2O$ at pH 1.8 (BR buffer) was added to the electrode surface, which was then air dried. The film was then covered by 10 μL of Nafion® solution (5 wt% in alcohol). Next, the modified electrode was transferred to the deaerated electrolyte solution in order to carry out the electrochemical and electrocatalytic experiments. When the modified electrode was not in use, it was left immersed in the supporting electrolyte.

2.3 Electrochemical measurements

Electrochemical measurements were carried out with a conventional three-electrode electrochemical cell. A Bioanalytical potentiostat (Model CV-50 W) controlled by a computer and a rotating disk electrode system (Model RDE-1, Bioanalytical Systems, Inc., West Lafayette, Indiana, USA) were used for electrochemical measurements. A glassy carbon electrode, diameter 3.0 mm, obtained from Bioanalytical Systems, Inc., was used as the working electrode, and Ag/AgCl and platinum were used as the reference and counter electrodes, respectively. All measurements were carried out at room temperature.

3 Results and discussion

3.1 Electrochemical formation and structure of Ru(HCF) film

The Ru(HCF) film was formed in the cyclic voltammetric scanning process. Chen et al. [23] proposed that this film is formed by deposition in the potential range of 0.2 to 1.1 V, followed by initial deposition at 1 V in the first positive scan. Ru^{4+} and RuO_2 were found to be the initiator and intermediate, respectively, for the formation of the film. Since, it is commonly recognized that the film should be constructed of oxo-bridges, the following reactions could occur in the potential cycling process if an acidic electrolyte is used:

$$Ru^{3+} \rightarrow Ru^{4+} + e^- \quad \text{(I)}$$

$$Ru^{4+} + 2H_2O \rightarrow Ru^{IV}O_2 + 4H^+ \quad \text{(II)}$$

The $Ru^{IV}O_2$ could then form an oxo-bridge with Fe(CN):

$$Ru^{IV}O_2 + \left[Fe^{III}(CN)_6\right]^{3-} + 3H^+ \rightarrow \left[Ru^{IV}-(OH)-Fe^{III}(CN)_6\right] + H_2O \quad \text{(III)}$$

In addition, a CN-based bridge structure [Ru^{III}–NC–$Fe^{III}(CN)_5]^0$) could also be formed through Reaction (IV), according to the literature [24, 25]:

$$Ru^{3+} + \left[Fe(CN)_6\right]^{3-} \rightarrow \left[Ru^{III}\text{–}NC\text{–}Fe^{III}(CN)_5\right]^{0} \quad \text{(IV)}$$

Thus, the Ru(HCF) film that we generated contained both Ru–O–Fe and Ru–NC–Fe bridges.

3.2 Electrochemical behavior of the Ru(HCF) film

Figure 1 shows the steady-state cyclic voltammograms in the potential range of –0.4–1.2 V versus Ag/AgCl, recorded on a glassy carbon electrode before and after modification with ruthenium (III) hexacyanoferrate in N_2-purged pH 1.8 BR solution. For the bare electrode, no redox process was observable in this potential range, and the CV response looks like a straight line along the x-axis with a current of around 0 (Fig. 1a). However, after the electrode was modified, four well-defined redox processes around –0.08, 0.53, 0.86, and 1.01 V could be observed (Fig. 1b). This is in good agreement with the literature [18, 23]. All of these waves were identified in the literature as one-electron processes [23]; the wave assignments are as follows:

Peak I, near –0.08 V, can be assigned to redox couple $[Ru^{II}\text{–}(OH)\text{–}Fe^{II}(CN)_6]^{3-}/[Ru^{III}\text{–}(OH)\text{–}Fe^{II}(CN)_6]^{2-}$; Peak II, near 0.53, to redox couple $[Ru^{III}\text{–}NC\text{–}Fe^{II}(CN)_5]^{-}/[Ru^{III}\text{–}NC\text{–}Fe^{III}(CN)_5]$ [17, 18, 24]; Peak III, around 0.86 V, to redox couple $[Ru^{III}\text{–}(OH)\text{–}Fe^{II}(CN)_6]^{2-}/[Ru^{III}\text{–}(O)\text{–}Fe^{III}(CN)_6]^{2-}$; and Peak IV, near 1.01 V, to redox couple $[Ru^{III}\text{–}(OH)\text{–}Fe^{III}(CN)_6]^{-}/[Ru^{IV}\text{–}(O)\text{–}Fe^{III}(CN)_6]^{-}$.

The surface behavior of the Ru(HCF) was confirmed by changing the scan rate of the electrode potential. All four redox peak currents increased linearly along with the increasing potential scan rate, indicating that the electrochemical behaviors of these surface redox processes follow a theoretically expected thin-layer pattern [26]. For redox in a thin layer or a surface adsorption layer, the reversible redox peak current is given by Eq. 1:

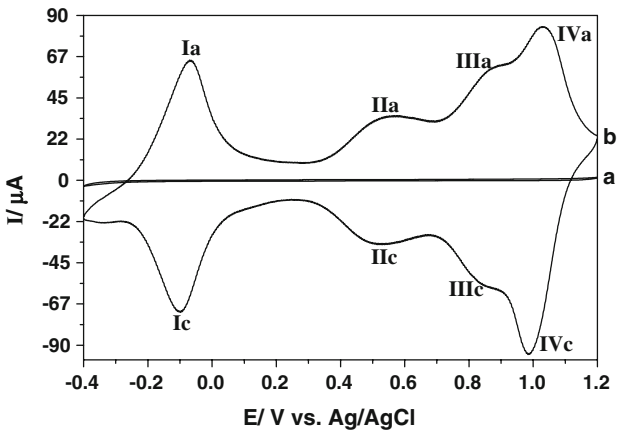

Fig. 1 Cyclic voltammograms obtained from (*a*) bare electrode and (*b*) glassy carbon electrode modified with ruthenium (III) hexacyanoferrate film in BR aqueous buffer solution (pH = 1.8) saturated with N_2. Potential scan rate: 100 mV s^{-1}

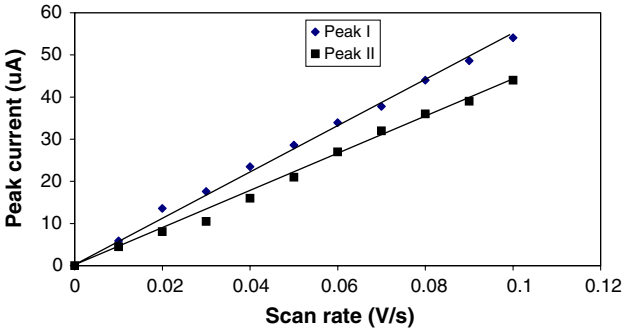

Fig. 2 Peak currents of wave Ia/Ic and wave IIa/IIc in Fig. 1, as a function of electrode potential scan rate. Experimental conditions are the same as for Fig. 1

$$I_p = \frac{n^2F^2Av\Gamma_i}{4RT} \quad (1)$$

where n is the electron transfer number involved in the electrochemical reaction of the individual redox process of Ru(HCF) film, F is the Faraday constant, R is the gas constant, T is the temperature, A is the electrode area, v is the electrode potential scan rate, and Γ_i is the surface concentration of the individual redox species.

From the slope of I_p versus v, either the surface concentration of the individual redox species or the electron transfer number of this redox species can be obtained. In order to obtain the surface concentrations of both metals in the film, the redox waves Ia/Ic and IIa/IIc were selected for ruthenium and iron, respectively. The peak currents of waves Ia/Ic and IIa/IIc as a function of the potential scan rate are shown in Fig. 2. The slopes of both linear lines can be obtained. According to Eq. 1, these two slopes can be used to determine the surface concentrations of iron and ruthenium in the Ru(HCF) film: 6.5×10^{-9} mol cm^{-2} for iron and 8.3×10^{-9} mol cm^{-2} for ruthenium. These results indicate that there are almost equal amounts of Ru–O–Fe and Ru–NC–Fe in the film. Considering the amounts of iron and ruthenium coated on the surface at the beginning of the preparation, it appears that only 10% of the iron and the ruthenium formed a film on the electrode, while the remaining 90% was dissolved in the solution.

3.2.1 Effect of pH on the electrochemical response of Ru(HCF)

The formal potentials of the peaks in Fig. 1 were obtained by averaging anodic and cathodic peak potentials. The pH dependencies of these formal potentials were recorded in a pH range of 1.8–7.0. For waves Ia/Ic and IIa/IIc, no significant pH dependency could be observed. However, the formal potentials of waves IIIa/IIIc and IVa/IVc, both showed pH dependencies. Using the linear plots of formal potential versus pH, as shown in Fig. 3, slopes for these

two pH-dependent waves were obtained: –69 mV/pH and –76 mV/pH, respectively. These values are close to the theoretical value of –59 mV/pH for a process involving a unit ratio of electrons to protons. The corresponding reactions for these four waves of Ru(HCF) film are proposed to be as follows:Wave Ia/Ic:

$$\left[\mathrm{Ru^{II}}-(\mathrm{OH})-\mathrm{Fe^{II}}(\mathrm{CN})_6\right]^{3-} \leftrightarrow \left[\mathrm{Ru^{III}}-(\mathrm{OH})-\mathrm{Fe^{II}}(\mathrm{CN})_6\right]^{2-} + \mathrm{e}^- \quad \text{(V)}$$

Wave IIa/IIc:

$$\left[\mathrm{Ru^{III}}-\mathrm{NC}-\mathrm{Fe^{II}}(\mathrm{CN})_5\right]^- \leftrightarrow \left[\mathrm{Ru^{III}}-\mathrm{NC}-\mathrm{Fe^{III}}(\mathrm{CN})_5\right] + \mathrm{e}^- \quad \text{(VI)}$$

Wave IIIa/IIIc:

$$\left[\mathrm{Ru^{III}}-(\mathrm{OH})-\mathrm{Fe^{II}}(\mathrm{CN})_6\right]^{2-} \leftrightarrow \left[\mathrm{Ru^{III}}-\mathrm{O}-\mathrm{Fe^{III}}(\mathrm{CN})_6\right]^{2-} + \mathrm{H}^+ + \mathrm{e}^- \quad \text{(VII)}$$

Wave IVa/IVc:

$$\left[\mathrm{Ru^{III}}-(\mathrm{OH})-\mathrm{Fe^{III}}(\mathrm{CN})_6\right]^- \leftrightarrow \left[\mathrm{Ru^{IV}}-\mathrm{O}-\mathrm{Fe^{III}}(\mathrm{CN})_6\right]^- + \mathrm{H}^+ + \mathrm{e}^- \quad \text{(VIII)}$$

In Reactions V and VI, no proton is involved, while in Reactions VII and VIII, one proton is involved and one electron transferred.

In addition, it was also observed that all four wave areas decreased with increasing solution pH, suggesting that the Ru(HCF) film was not stable in less acidic solutions. It was confirmed that the most stable surface film could be obtained at a pH of 1.8. Therefore, the following results for hydrazine oxidation were all obtained at pH 1.8.

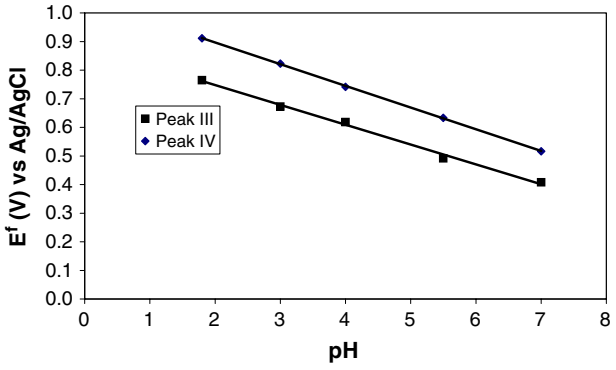

Fig. 3 Formal potential as a function of pH. Cyclic voltammograms were recorded on a glassy carbon electrode modified with ruthenium (III) hexacyanoferrate, in a N_2-saturated BR aqueous buffer solution at different pHs: 1.8, 3.0, 4.0, 5.5, and 7.0. Potential scan rate: 100 mV s^{-1}

3.3 Electrocatalytic response toward hydrazine oxidation

Figure 4 shows a cyclic voltammogram for a glassy carbon electrode modified with Ru(HCF), recorded in a 1.8 pH solution in the presence of hydrazine. For comparison, the same electrode was also used to record a cyclic voltammogram under similar conditions but without hydrazine in the solution. It can be seen that in the presence of hydrazine, a large oxidation peak appeared at 0.96 V, indicating that the Ru(HCF) film had electrocatalytic activity toward hydrazine oxidation. A bare glassy carbon electrode was also tested in the same hydrazine-containing solution but no such oxidation wave was observed at 0.96 V, further confirming that the hydrazine oxidation activity was due to the presence of Ru(HCF) film on the electrode surface. It has been reported that both redox couples of waves III and IV can be active catalytic sites for ethanol electrooxidation [23]. We believe that these two active catalytic sites were also responsible for the electrooxidation of hydrazine.

From Fig. 4, it can also be observed that wave I became much smaller when hydrazine was present in the solution. This could suggest that hydrazine molecules are bound to an Ru center, deactivating the redox reactions of $[\mathrm{Ru^{II}}–(\mathrm{OH})–\mathrm{Fe^{II}}(\mathrm{CN})_6]^{3-}/[\mathrm{Ru^{III}}–(\mathrm{OH})–\mathrm{Fe^{II}}(\mathrm{CN})_6]^{2-}$ couples; when the electrode potential is further increased, the hydrazine-bound Ru center is converted from Ru(III)-(NH_2NH_2) to Ru(IV)-(NH_2NH_2), then the bound hydrazine molecules start to lose electrons to the metal centers. Similar depression was also observed with wave IIIa, suggesting that hydrazine molecules are also bound to an Fe center. We thus believe that the Ru(IV) and Fe(III) centers are the catalytically active sites for hydrazine oxidation.

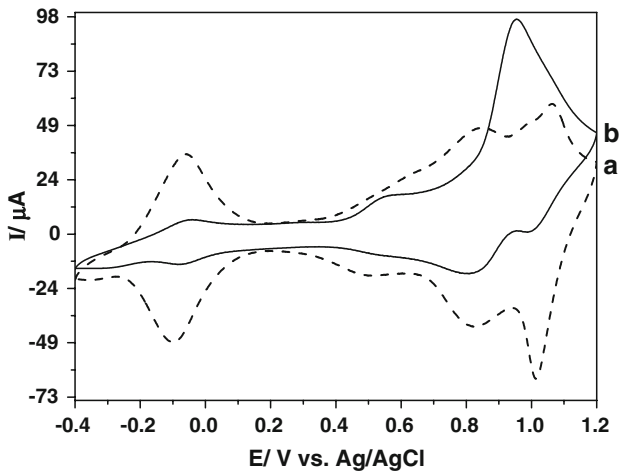

Fig. 4 Cyclic voltammograms obtained using a glassy carbon electrode modified with ruthenium (III) hexacyanoferrate film in N_2-saturated BR aqueous buffer solution (pH = 1.8), in the absence (*a*) and presence (*b*) of 1×10^{-3} mol L^{-1} of hydrazine. Potential scan rate: 100 mV s^{-1}

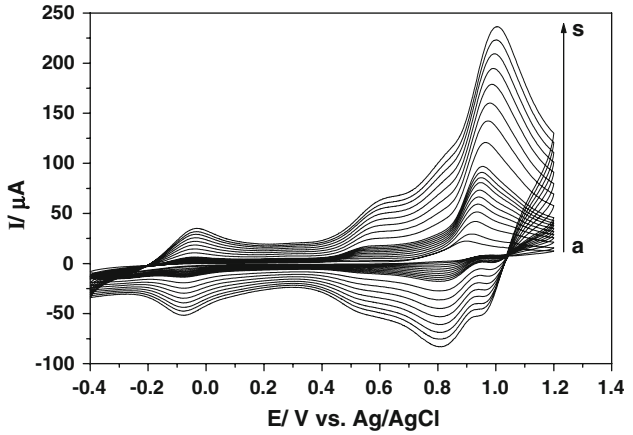

Fig. 5 Cyclic voltammograms at different potential scan rates, recorded using a glassy carbon electrode coated with ruthenium (III) hexacyanoferrate in N_2-saturated BR aqueous buffer solution (pH = 1.8) containing 1×10^{-3} mol L^{-1} of hydrazine. (*a*) 5, (*b*) 10, (*c*) 20, (*d*) 30, (*e*) 40, (*f*) 50, (*g*) 60, (*h*) 70, (*i*) 80, (*j*) 90, (*k*) 100, (*l*) 150, (*m*) 200, (*n*) 250, (*o*) 300, (*p*) 350, (*q*) 400, (*r*) 450, and (*s*) 500 mV s^{-1}

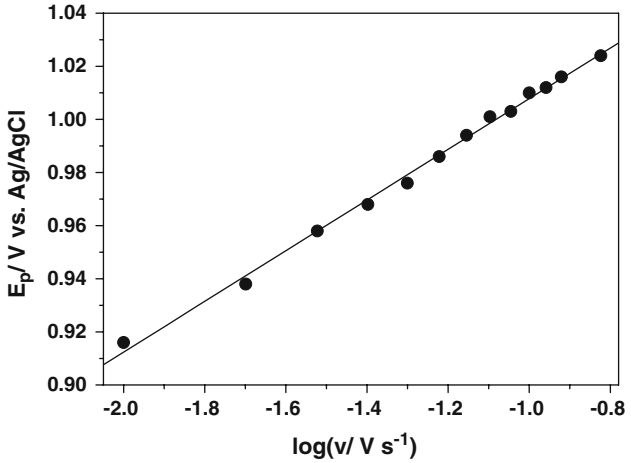

Fig. 6 Peak potential as a function of the logarithm of the potential scan rate for hydrazine oxidation on a glassy carbon electrode coated with ruthenium (III) hexacyanoferrate. Data from Fig. 5

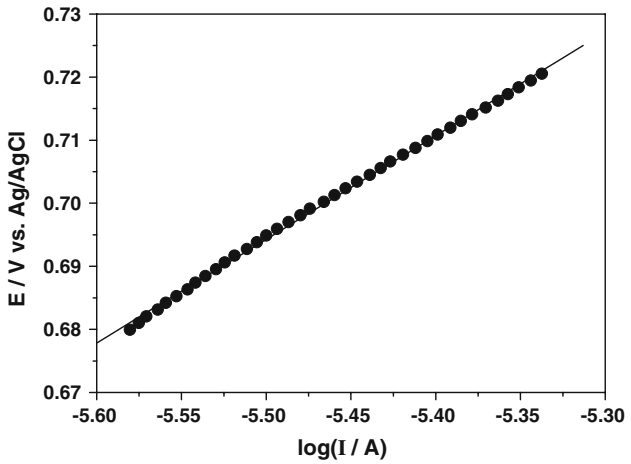

Fig. 7 Tafel plot for a glassy carbon electrode modified with ruthenium (III) hexacyanoferrate film, in BR buffer aqueous solution (pH = 1.8) containing 1×10^{-3} mol L^{-1} hydrazine. Data from Fig. 5

Cyclic voltammograms for hydrazine oxidation were also recorded at different potential rates, as shown in Fig. 5. It can be observed that the peak current of hydrazine oxidation at 0.96 V increased linearly with the square root of the potential scan rate, suggesting an irreversible diffusion-limited electrochemical process [26].

From Fig. 5, it can also be observed that the hydrazine oxidation peak potential shifts to a positive value as scan rate increases, suggesting a kinetically limited reaction between the active site of the Ru(HCF) film and hydrazine [20]. The plot between the peak potential versus the logarithm of the scan rate shows a linear relationship with a slope of 95 mV/dec (Fig. 6). According to the literature [10, 25, 26], this linear relationship can be expressed as Eq. 2:

$$E_P = K + \frac{2.303RT}{2\alpha n_\alpha F}\log v \tag{2}$$

where E_p is the peak potential of hydrazine oxidation, K is a constant, R and T have their usual significance as defined in Eq. 1, α is the transfer coefficient for hydrazine oxidation, n_α is the electron transfer number involved in the rate determining step of hydrazine oxidation, and v is the potential scan rate. From the slope, an αn_α value of 0.31 can be calculated.

The αn_α value could also be calculated using the Tafel slope obtained from the relationship between the electrode potential and the logarithmic current (E–logI plot). Figure 7 shows the Tafel plot constructed from the cyclic voltammogram at 5.0 mV s^{-1}, obtained from Fig. 5. A linear relationship can be observed in the low potential region, with a slope of 164 mV/dec. The Tafel plot can be expressed as follows:

$$E = a + \frac{2.303RT}{\alpha n_\alpha F}\log(I) \tag{3}$$

where E is the electrode potential, I is the current of hydrazine oxidation, α and n_α were defined in Eq. 2, and R, T, and F have their previously defined meanings. Based on Eq. 3 and the measured Tafel slope (164 mV/dec), an αn_α of 0.36 can be obtained. This value is close to what was obtained from Fig. 6 (0.31), and is also in agreement with what was reported for hydrazine oxidation on other catalyst films [10].

3.3.1 *Effect of pH on the electrocatalytic oxidation of hydrazine*

In order to investigate the effect of pH on catalyzed hydrazine oxidation, cyclic voltammograms were also

recorded in hydrazine-containing solutions with different pHs. The half-wave potential ($E_{P/2}$) of the hydrazine oxidation peak was plotted as a function of pH, as shown in Fig. 8. A linear relationship can be observed, with a slope of 76 mV/pH in the range of 1.8–5.0. This value could suggest a process in which one proton is transferred for each transferred electron. If the overall reaction of hydrazine is a four-electron process, the reaction could be written as follows:

$$N_2H_4 \rightarrow N_2 + 4H^+ + 4e^- \quad \text{(IX)}$$

3.3.2 *Hydrazine oxidation kinetics evaluated by rotating disk electrode experiments*

In order to more quantitatively evaluate the kinetics of hydrazine oxidation catalyzed by Ru(HCF), a rotating glassy carbon disk electrode coated by Ru(HCF) film was tested in a hydrazine-containing solution. The current–potential curves obtained at different rotating rates in a 1.8 pH BR buffer solution containing 5×10^{-4} mol L^{-1} hydrazine are shown in Fig. 9. Plateau currents can be observed for all rotation rates. These limiting currents can be used to obtain the overall electron numbers transferred in hydrazine oxidation, and the Koutecky–Levich theory can be used to express the current–potential curves in Fig. 9:

$$1/I_{\text{lim}} = 1/I_{\text{lev}} + 1/I_{\text{k}} \quad (4)$$

where I_{lim} is the plateau current, I_{k} is the kinetic current, and I_{lev} is the Levich diffusion current, which can be expressed as:

$$I_{\text{lev}} = 0.201nFAC_{\text{hyrazine}}D_{\text{hydrazine}}^{2/3}\gamma^{-1/6}\omega^{1/2} \quad (5)$$

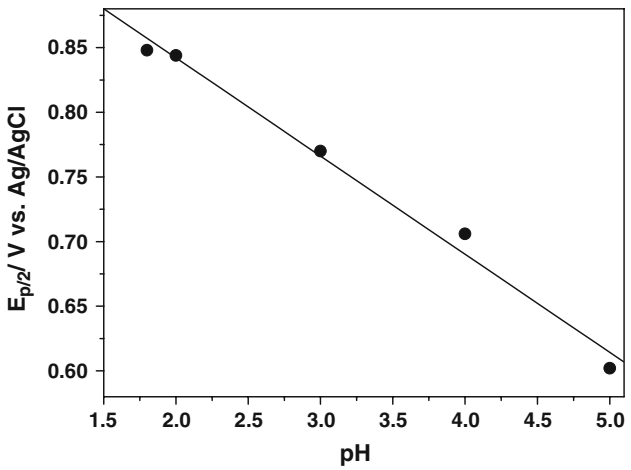

Fig. 8 Half-wave potential ($E_{P/2}$) as a function of solution pH. Data from cyclic voltammograms obtained from a glassy carbon electrode modified with ruthenium (III) hexacyanoferrate film, in a N_2-saturated BR aqueous buffer solution (pH = 1.8) containing 1×10^{-3} mol L^{-1} hydrazine

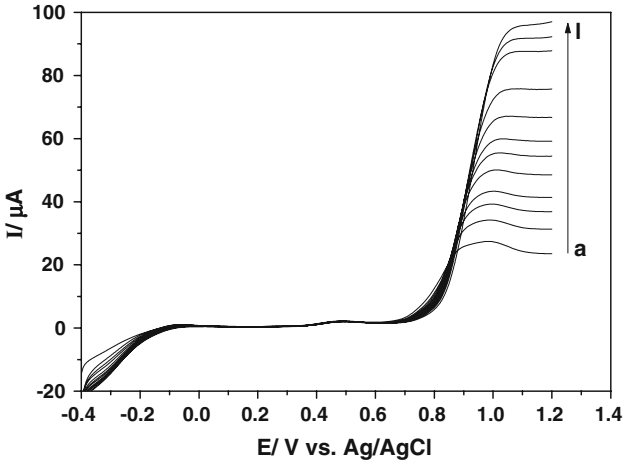

Fig. 9 Current–potential curves as a function of electrode rotating rate, recorded using a rotating glassy carbon electrode coated with ruthenium (III) hexacyanoferrate film, in a N_2-saturated BR buffer aqueous solution (pH = 1.8) containing 5×10^{-4} mol L^{-1} hydrazine. Potential scan rate: 5 mV s^{-1}. The electrode rotating rates from a to l are (*a*) 50, (*b*) 100, (*c*) 150, (*d*) 200, (*e*) 300, (*f*) 400, (*g*) 500, (*h*) 700, (*i*) 1,000, (*j*) 1,600, (*k*) 2,000, and (*l*) 3,000 rpm

where n, $D_{\text{hydrazine}}$, and $C_{\text{hydrazine}}$ are the overall electron transfer number (=4 for hydrazine oxidation to N_2), the diffusion coefficient, and the concentration of hydrazine, respectively; γ is the kinetic viscosity of the electrolyte solution; and ω is the rotation rate.

A plot of $1/I_{\text{lim}}$ versus $\omega^{-1/2}$ is shown in Fig. 10, together with a theoretical four-electron line for comparison. The theoretical line was calculated according to Eqs. 4 and 5 for a four-electron hydrazine oxidation process, using the following parameters: $D = 1.4 \times 10^{-5}$ cm^2 s^{-1} [17, 18], $C = 5 \times 10^{-7}$ mol cm^{-3}, $v = 1.02 \times 10^{-2}$ cm^2 s^{-1}, $n = 4$, and $I_{\text{k}} = \infty$. It can be seen that the experimental line is approximately parallel to the calculated one, indicating that catalyzed hydrazine oxidation is a four-electron process,

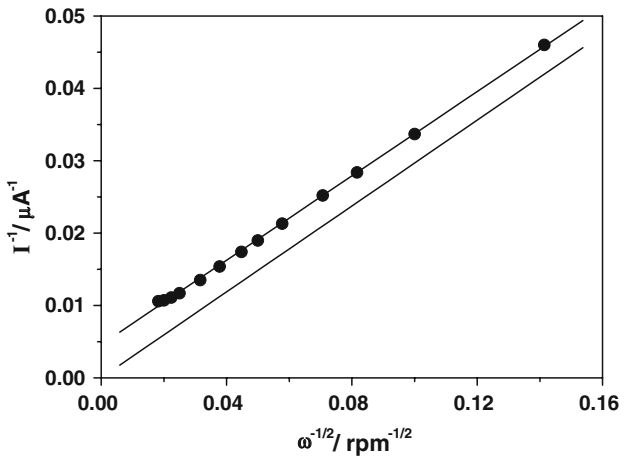

Fig. 10 Koutecky–Levich plots (experimental and theoretical) for hydrazine oxidation electrocatalyzed by ruthenium (III) hexacyanoferrate film on a glassy carbon electrode. Data from Fig. 9

producing N_2. Therefore, the overall oxidation of hydrazine in an acidic solution, expressed as Reaction (IX), is further confirmed.

The kinetic current I_k can be expressed as Eq. 6:

$$I_k = nFAK_{\text{hydrazine}}C_{\text{hydrazine}}\Gamma_{\text{Ru(HCF)}} \quad (6)$$

where $K_{\text{hydrazine}}$ is the rate constant of the chemical reaction that limits the plateau current, $\Gamma_{\text{Ru(HCF)}}$ is the surface concentration of Ru(HCF) catalyst, and the other terms have their usual significance as described earlier. I_k can be obtained from the intercept of the Koutecky–Levich line in Fig. 10. The rate constant $K_{\text{hydrazine}}$ obtained for the electrocatalyzed hydrazine oxidation was calculated to be 1.8×10^6 mol^{-1} cm^3 s^{-1}.

3.3.3 Reaction mechanism discussion

Based on the discussion of Fig. 4, the initial step for hydrazine oxidation on the catalyst centers should be the bonding process between the hydrazine molecules and the Ru(IV) and Fe(III) centers to form adducts, followed by electron transfer to form the product. As hydrazine contains protons, proton transfer must be involved in the transfer of electrons. As shown in Fig. 8, the half-wave potential ($E_{P/2}$) of the hydrazine oxidation peak was obtained as a function of pH. A linear relationship between $E_{P/2}$ and pH was observed, with a slope of 76 mV/pH in the range of 1.8–5.0. This value could suggest a process of one-to-one electron–proton transfer.

Based on the above information and the literature [23], the mechanism of hydrazine oxidation catalyzed by Ru(HCF) is proposed as follows:

$$\left[Ru^{III}-(OH)-Fe^{III}(CN)_6\right]^- \leftrightarrow \left[Ru^{IV}-O-Fe^{III}(CN)_6\right]^- + H^+ + e^- \quad \text{(VIII)}$$

$$\left[Ru^{IV}-O-Fe^{III}(CN)_6\right]^- + N_2H_4 \rightarrow \left[N_2H_3-Ru^{IV}-O-Fe^{III}(CN)_6\right]^- + H^+ + e^- \quad \text{(X)}$$

$$\left[N_2H_3-Ru^{IV}-O-Fe^{III}(CN)_6\right]^- \rightarrow \left[Ru^{III}-(OH)-Fe^{III}(CN)_6\right]^- + N_2 + 2H^+ + 3e^- \quad \text{(XI)}$$

The $[Ru^{III}–(OH)–Fe^{III}(CN)_6]^-$ formed in Reaction XI will lose one electron and one proton on the electrode through Reaction VIII, forming the reaction cycle.

4 Conclusions

A (Ru(HCF)) film coated on a glassy carbon electrode was explored as an electrocatalyst for hydrazine oxidation. Surface cyclic voltammograms recorded using the coated electrode in a N_2-saturated electrolyte solution and in the absence of hydrazine showed four reversible one-electron redox waves (Ia/Ic, IIa/IIc, IIIa/IIIc, and IVa/IVc, respectively), which could be assigned to the redox couples $[Ru^{II}–(OH)–Fe^{II}(CN)_6]^{3-}/[Ru^{III}–(OH)–Fe^{II}(CN)_6]^{2-}$, $[Ru^{III}–NC–Fe^{II}(CN)_6]^{2-}/[Ru^{III}–NC–Fe^{III}(CN)_6]^-$, $[Ru^{III}–(OH)–Fe^{II}(CN)_6]^{2-}/[Ru^{III}–(O)–Fe^{III}(CN)_6]^{2-}$, and $[Ru^{III}–(OH)–Fe^{III}(CN)_6]^-/[Ru^{IV}–(O)–Fe^{III}(CN)_6]^-$, respectively. Experiments with different pH solutions showed that the wave potentials of both Ia/Ic and IIa/IIc were independent of pH, while the other two waves (IIIa/IIIc and IVa/IVc) were pH-dependent. The plots of wave potential versus pH for both IIIa/IIIc and IVa/IVc indicated that these two redox processes involved one proton being transferred per electron.

It was observed that the Ru(HCF)-modified electrode exhibited strong electrocatalytic activity toward hydrazine oxidation in acidic media. The catalytically active sites were identified as the Ru(IV) center in $[Ru^{IV}–O–Fe^{III}(CN)_6]^-$ and the Fe(III) center in $[Ru^{III}–(OH)–Fe^{III}(CN)_6]^-$ inside the Ru(HCF) film, which bound with hydrazine to form adducts for further oxidation. The potential scan rate dependency of the peak current of hydrazine oxidation, shown by cyclic voltammograms recorded using a Ru(HCF)-coated electrode in a solution containing hydrazine, revealed that electrooxidation was a diffusion-controlled process. Kinetic studies using potential scan rate dependency, Tafel plots, and rotating disk electrode technique showed that the catalyzed hydrazine oxidation was a complete four-electron/four-proton process producing N_2, and the rate determining step might be a one-electron process with a transfer coefficient (α) of around 0.31–0.36. In addition, based on kinetic analysis and the literature, a possible reaction mechanism for catalyzed hydrazine oxidation was proposed to facilitate further understanding.

Acknowledgments The authors gratefully acknowledge the support of the CNPq, FAPEMA, PETROBRAS, and the Institute for Fuel Cell Innovation, National Research Council of Canada.

References

1. Vernot EH, MacEwen JD, Bruner RH, Haus CC, Kinkead ER (1985) Fund Appl Toxicol 5:1050
2. Ardakani MM, Karami PE, Rahimi P, Zare HR, Naeimi H (2007) Electrochim Acta 52:6118
3. Golabi SM, Zare HR (1999) J Electroanal Chem 465:168
4. Golabi SM, Noor-Mohammadi F (1998) J Solid State Electrochem 2:30
5. Golabi SM, Zare HR, Hamzehloo M (2001) Microchem J 69:13
6. Wang J, Golden T, Li R (1988) Anal Chem 60:1642
7. Hou W, Hua J, Wang E (1991) Chin Sci Bull 36:785
8. Lin C, Bocarsly AB (1991) J Electroanal Chem 300:325
9. Zare HR, Nasirzadeh N (2006) Electroanalysis 18:507
10. Abbaspour A, Kamyabi MA (2005) J Electroanal Chem 576:73
11. Ensafi AA, Mirmomtaz E (2005) J Electroanal Chem 583:176
12. Pingarrón JM, Oritz Hernández I, González-Cortés A, Yáñez-Sedeño P (2001) Anal Chim Acta 439:281

13. Neff VD (1978) J Electrochem Soc 125:886
14. Cox JA, Kulesza PJ (1988) Anal Chem 5:1021
15. Cox JA (1987) J Electroanal Chem 233:87
16. Kulesza PJ (1987) J Electroanal Chem 220:295
17. Cataldi TRI, De Benedetto CE, Campa C (1998) J Electroanal Chem 458:149
18. Kasem K, Steldt FR, Miller TJ, Zimmerman AN (2003) Micropor Mesopor Mater 66:133
19. Cataldi TRI, De Benedetto GE, Bianchini A (1999) J Electroanal Chem 471:42
20. Shaidarova LG, Ziganshina SA, Tikhonova LN, Budnikov GK (2003) J Anal Chem 58:1144
21. Kulesza PJ, Jedral T, Galus Z (1998) Electrochim Acta 34:851
22. Kulesza PJ, Grzybowska B, Malik MA, Chojak M, Miecznikowski KJ (2001) J Electroanal Chem 512:110
23. Chen S-M, Lu M-F, Lin K-C (2005) J Electroanal Chem 579:163
24. Paixão TRLC, Bertotti M (2007) Electrochim Acta 52:2181
25. Cataldi TRI, Salvi AM, Centonze D, Sabbatini L (1996) J Electroanal Chem 406:91
26. Bard AJ, Faulkner LR (2001) Electrochemical methods: fundamentals and applications. Wiley, New York, p 236